Electronic Supplementary Material (ESI) for ChemComm.

Supporting Information

Heterostructured $ZnFe_2O_4$@Ni_3S_2 nanosheet arrays on Ni foam as an efficient oxygen evolution catalyst

Haiqing Liu, [a] *Juhong Miao,*[*a] *Yubin Wang,* [a] *Siyu Chen,* [a] *Yujia Tang* [a] *and Dongdong Zhu*[*a]

[a] School of Chemistry and Materials Science, Nanjing University of Information Science & Technology, Nanjing, 210044, China.
E-mail: miaojh_2008@163.com, dd.zhu@nuist.edu.cn

1. Experimental Section

1.1 Materials

Zinc(II) acetate anhydrous ($Zn(CH_3COO)_2$), iron(III) nitrate nonahydrate ($Fe(NO)_3·9H_2O$), thiourea (CH_4N_2S) and ammonium fluoride (NH_4F) were purchased from Sinpharm Chemical Reagent Co. Ltd, China. Urea (H_2NCONH_2) and Nickel(II) chloride hexahydrate ($NiCl_2·6H_2O$) were obtained from Aladdin Reagent Co. Ltd. Suzhou Sinero Technology Co., Ltd provided Nickel foam and RuO_2.

1.2 Synthesis of $ZnFe_2O_4$/NF

The successful growth of $ZnFe_2O_4$ nanosheets on nickel foam was synthesized by a typical hydrothermal method. Firstly, the nickel foam (2 cm × 4 cm) was ultrasonically cleaned with 3 M HCl and anhydrous ethanol for 10 min to remove surface oxides and oils. Then, 0.5 mmol of $Zn(CH_3COO)_2$, 1 mmol of $Fe(NO)_3·9H_2O$, 0.37 g of NH_4F, and 0.72 g of urea were dissolved in 30 mL of deionized water and stirred in an ultrasonic bath until a homogeneous clear solution was formed. The mixed solution and the pre-cleaned nickel foam substrate were transferred to a 50 mL sealed Teflon autoclave and reacted at 140 °C for 4 hours. The resulted Zn-Fe precursor/NF and precursor powder were rinsed with water and ethanol, respectively, and dried in an oven at 60 °C overnight. The above Zn-Fe precursor/NF and precursor powder were heated to 350 °C in a muffle furnace exposed to air and calcined for 2 h at a heating rate of 3 °C·min^{-1} to obtain $ZnFe_2O_4$/NF and $ZnFe_2O_4$ powder.

1.3 Synthesis of $ZnFe_2O_4$@Ni_3S_2/NF

$ZnFe_2O_4$@Ni_3S_2/NF was synthesized by an electrochemical deposition process in a simple three-electrode electrochemical system. The prepared $ZnFe_2O_4$/NF (1 × 2 cm^{-2}), platinum foil (1 × 1 cm^{-2}) and saturated Ag/AgCl were used as the working electrode, counter electrode, and reference electrode, respectively. The electrodeposition solution was obtained by dissolving 2 mmol $NiCl_2·6H_2O$ and 40 mmol CH_4N_2S in 50 mL of deionized water and mixed thoroughly. Ni_3S_2 nanosheets were electrochemically deposited on the $ZnFe_2O_4$ nanosheets surface using cyclic voltammetry with a potential range of -1.2 to 0.2 V, a scan rate of 5 mV s^{-1}, and different electrodeposition cycles of 5, 10, 20 and 30. The resulted $ZnFe_2O_4$@Ni_3S_2/NF electrodes were washed several times with water and dried at 60 °C for 12 h.

1.4 Synthesis of Ni_3S_2/NF

For comparison purpose, Ni_3S_2 was prepared using the same electrodeposition procedure on pre-cleaned unmodified nickel foam electrodes.

1.5 Synthesis of RuO_2/NF

The RuO_2 catalyst (20 mg) was first dispersed in a mixed solution with 1 mL of deionized water, 0.8 mL of anhydrous ethanol and 0.2 mL of 5 wt % Nafion solution. A homogeneous ink was formed after sonication for 30 min. Then, the prepared catalyst ink was dropped on a clean NF ($1 \times 1 cm^{-2}$).

1.6 Characterization

All prepared electrodes were characterized via morphology, composition, and electrochemical tests. The structure of the prepared electrodes was characterized by X-ray powder diffraction (XRD) technology using a powder X-ray diffractometer (Bruker Rigaku-Dmax 2500) with CuKα radiation (λ = 0.15418 nm) in the range from 5° to 80°. The microscopic morphology and dimension of the samples were obtained on field emission scanning electron microscopy (FE-SEM, ZEISS GeminiSEM 300) and field emission transmission electron microscope (TEM, FEI Tecnai G2 F30), respectively. X-ray photoelectron spectroscopy (XPS) was employed to measure the chemical state of the products at an ESCALABMK II x-ray photoelectron spectrometer with Mg as the excitation source.

1.7 Electrochemical characterization

The electrochemical performance was tested using a CHI 660E electrochemical workstation (Chenhua, Shanghai, China) and a three-electrode system. The working electrode was a prepared nickel foam composite electrode ($1 \times 1 cm^{-2}$), the reference electrode was a Hg/HgO (1 M KOH) electrode, and the counting electrode was a graphite rod electrode. All electrochemical tests were carried out in an electrolyte of 1 M KOH at room temperature and the potential values tested were calibrated according to the reversible hydrogen electrode E (RHE) = E (Hg/HgO) + 0.059pH + 0.098. After activation with a least of 100 turns of cyclic voltammetry (CV) scanning performed, cyclic voltammetry (CV), Linear sweep voltammetry (LSV), Chronopotentiometry (CP), electrochemical impedance spectroscopy (EIS), and double-layer capacitance (C_{dl}) were used to measure the electrochemical catalytic performance of OER, respectively. C_{dl} was evaluated by fitting the average anodic and cathodic current densities ($\Delta j = (j_a - j_c)/2$) at a voltage of -0.1 V (vs. Hg/HgO) to the scan rate. Polarization curves were recorded by linear sweep voltammetry at a scan rate of 2 mV s^{-1} after the CV curve had stabilized and were all compensated for by a 90% drop in iR.

2. Supplementary Figures and Tables

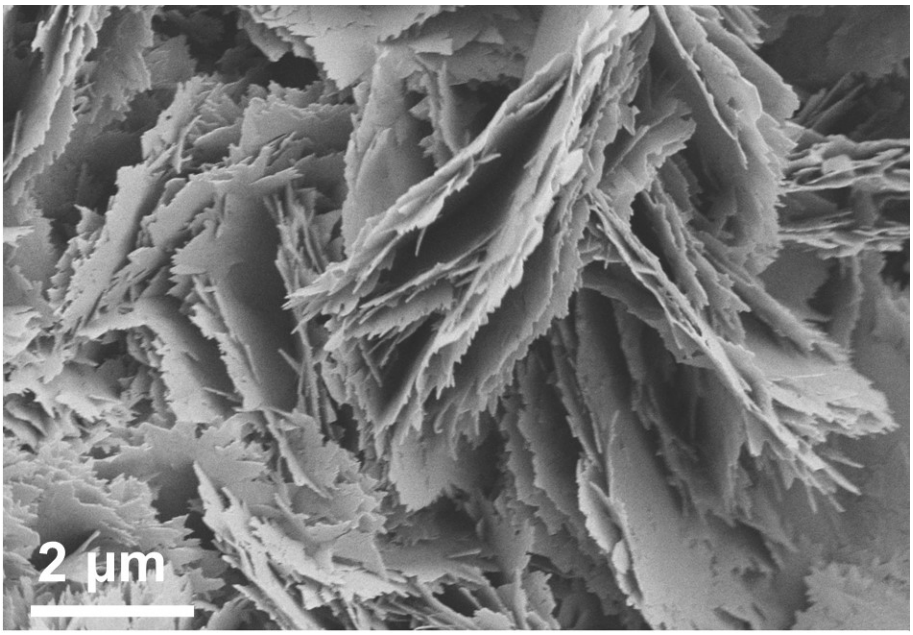

Figure S1. SEM image of Zn-Fe precursors/NF.

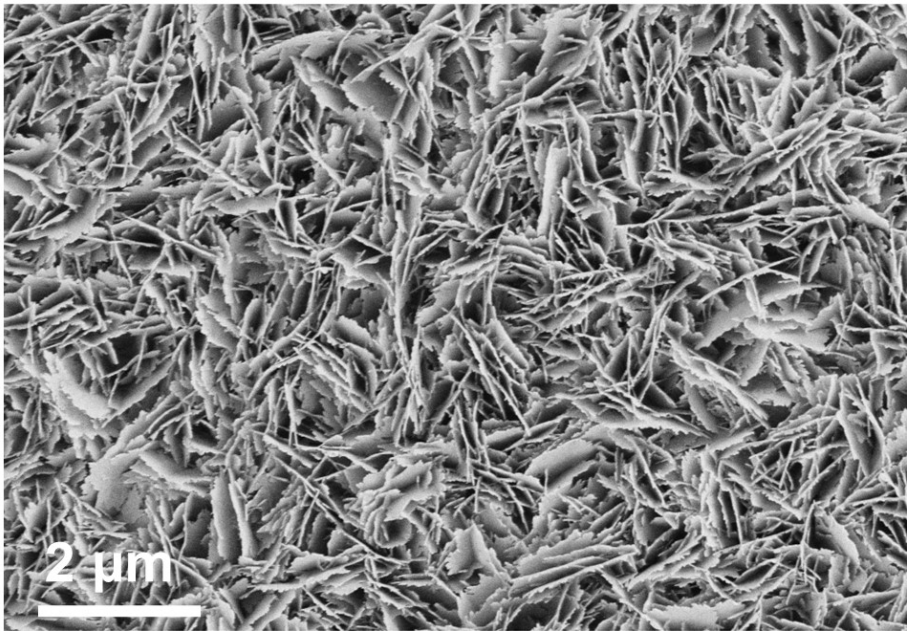

Figure S2. SEM image of $ZnFe_2O_4$/NF.

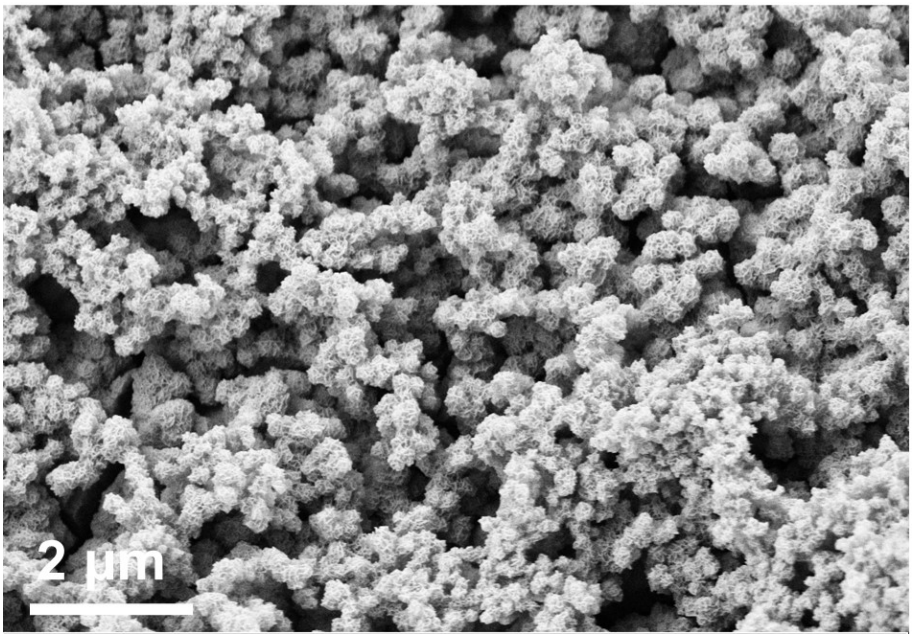

Figure S3. SEM image of Ni_3S_2/NF.

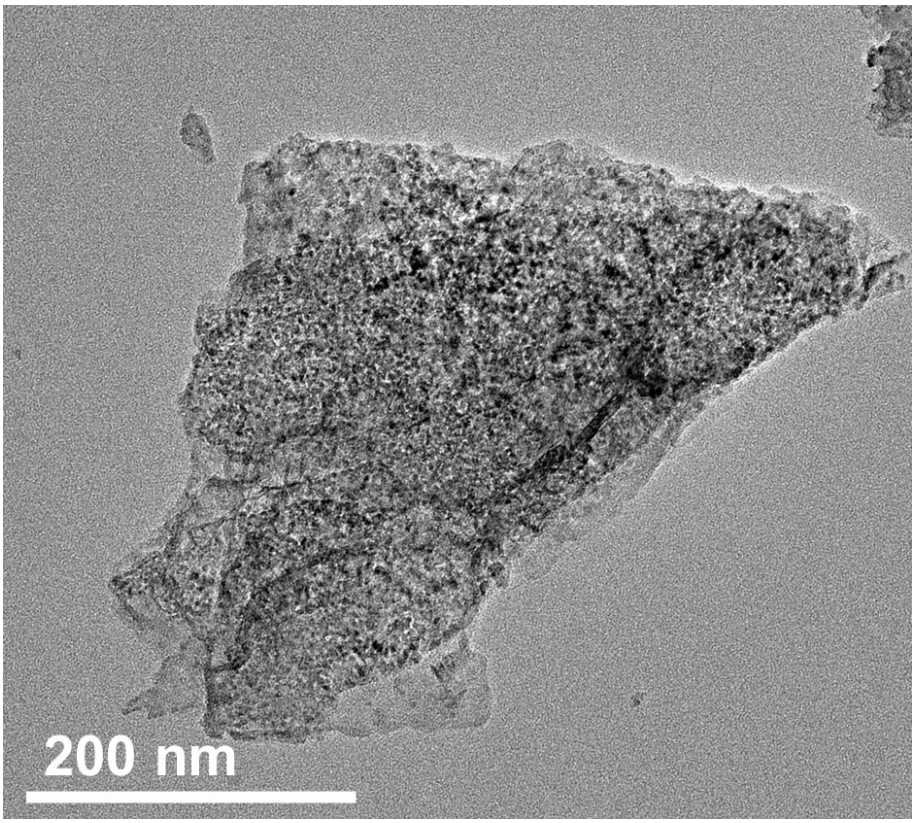

Figure S4. HRTEM image of $ZnFe_2O_4$@ Ni_3S_2/NF.

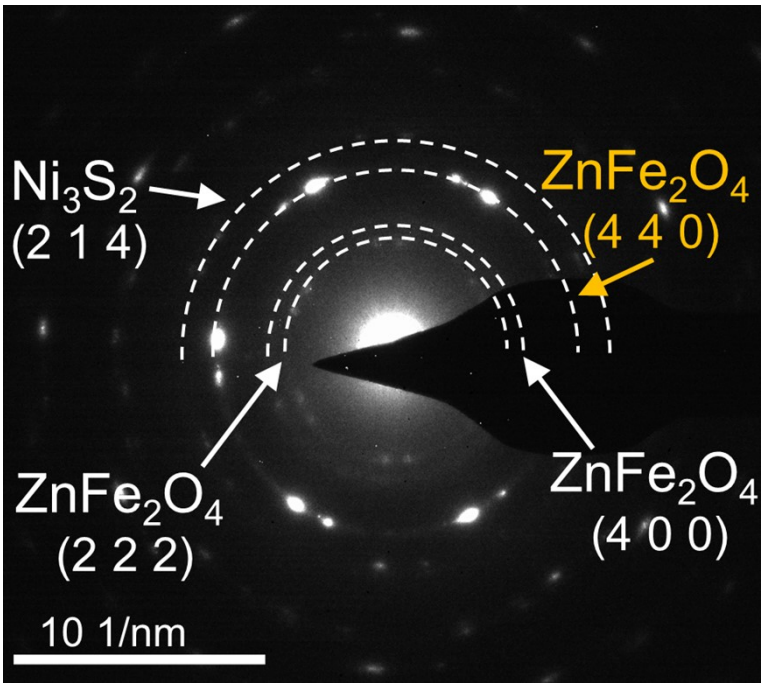

Figure S5. SAED pattern of $ZnFe_2O_4$@Ni_3S_2/NF.

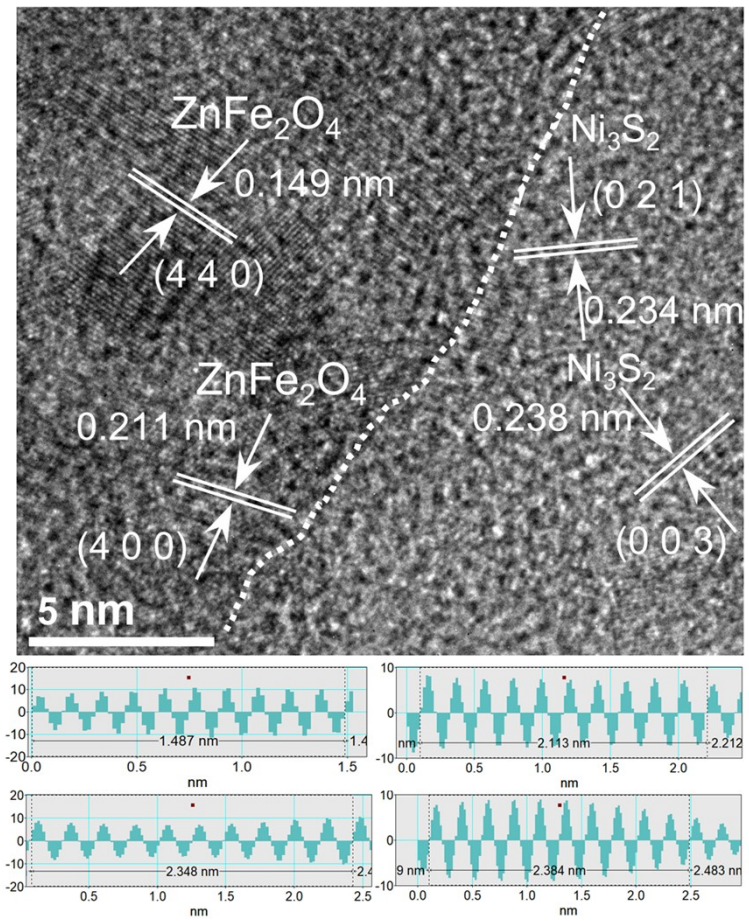

Figure S6. HRTEM image and corresponding profile of $ZnFe_2O_4$@Ni_3S_2/NF.

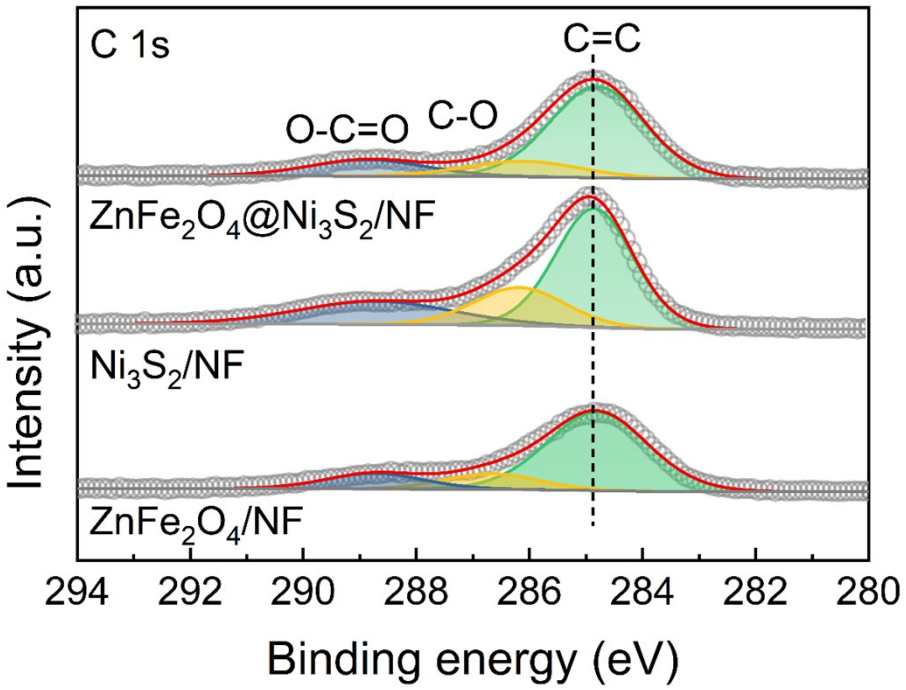

Figure S7. C 1s high-resolution spectra of the $ZnFe_2O_4$/NF, Ni_3S_2/NF and $ZnFe_2O_4$@Ni_3S_2/NF.

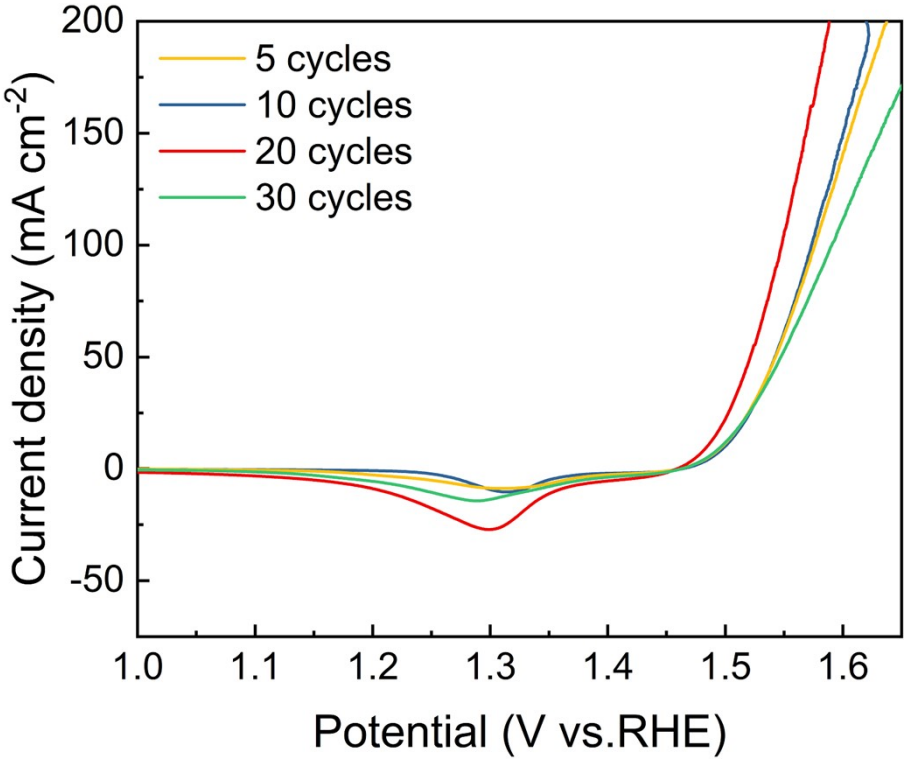

Figure S8. Polarization curves of $ZnFe_2O_4$@Ni_3S_2/NF at different electrodeposition cycle.

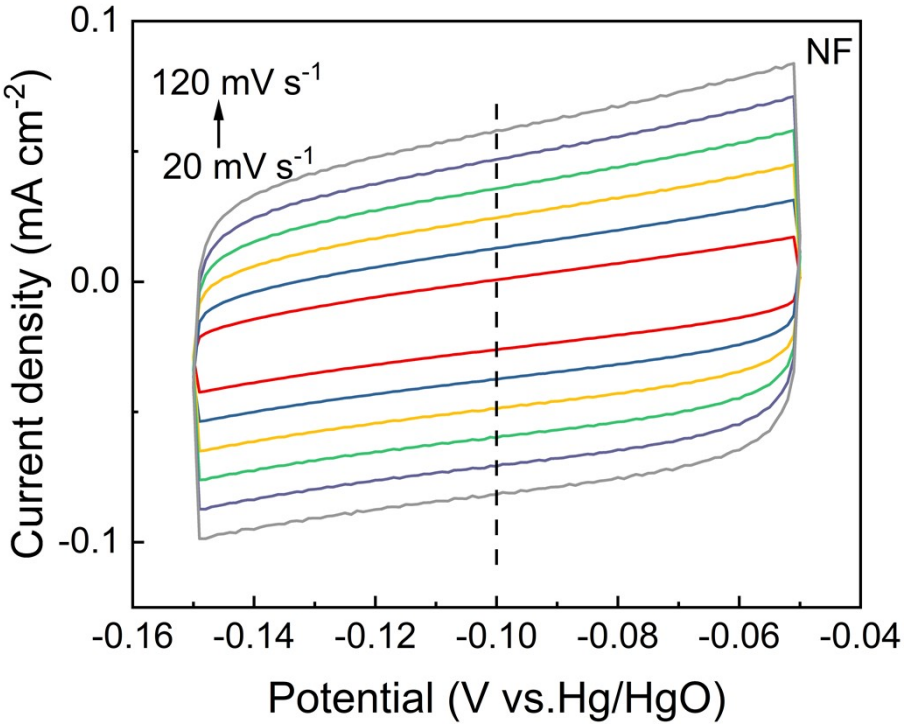

Figure S9. CV curves for NF at scan rates from 20 to 120 mV s^{-1}.

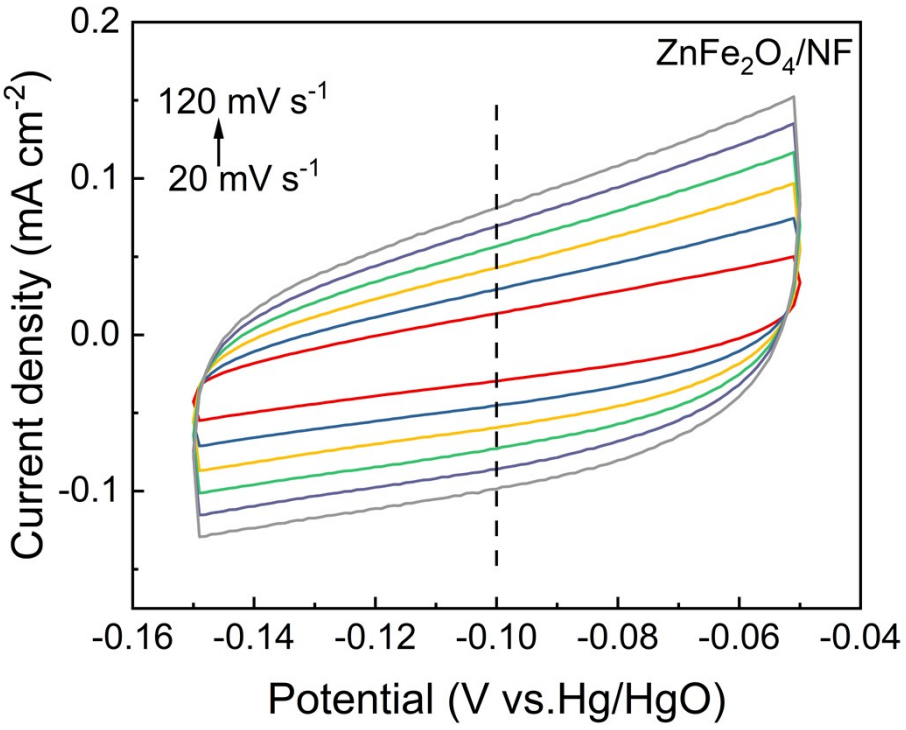

Figure S10. CV curves for $ZnFe_2O_4$/NF at scan rates from 20 to 120 mV s^{-1}.

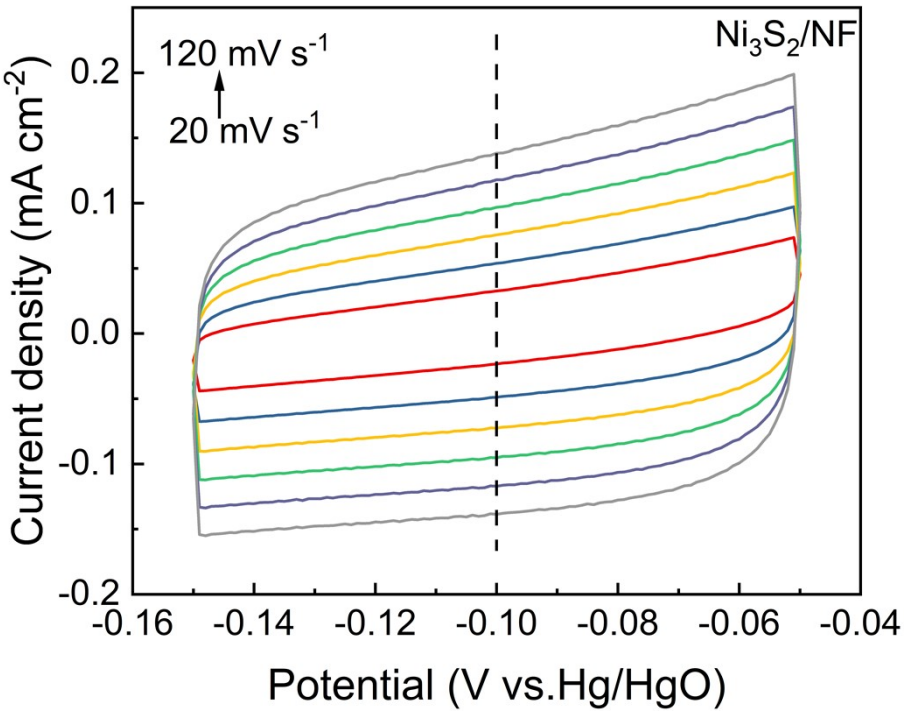

Figure S11. CV curves for Ni_3S_2/NF at scan rates from 20 to 120 mV s^{-1}.

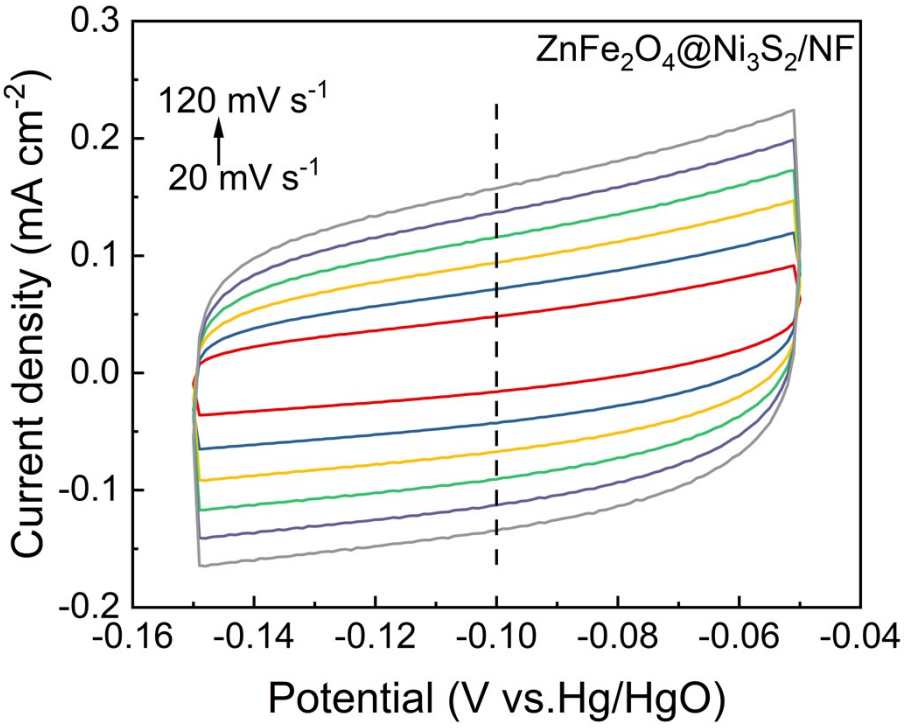

Figure S12. CV curves for $ZnFe_2O_4$@Ni_3S_2/NF at scan rates from 20 to 120 mV s^{-1}.

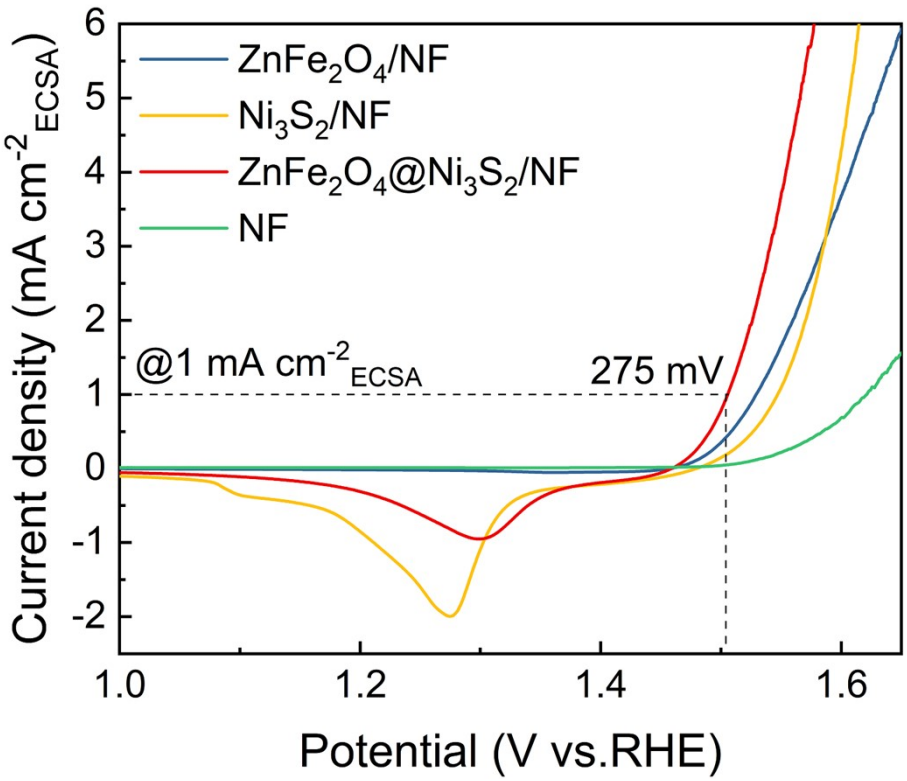

Figure S13. OER polarization curve of $ZnFe_2O_4$@Ni_3S_2/NF initial and after 1000 CV cycles.

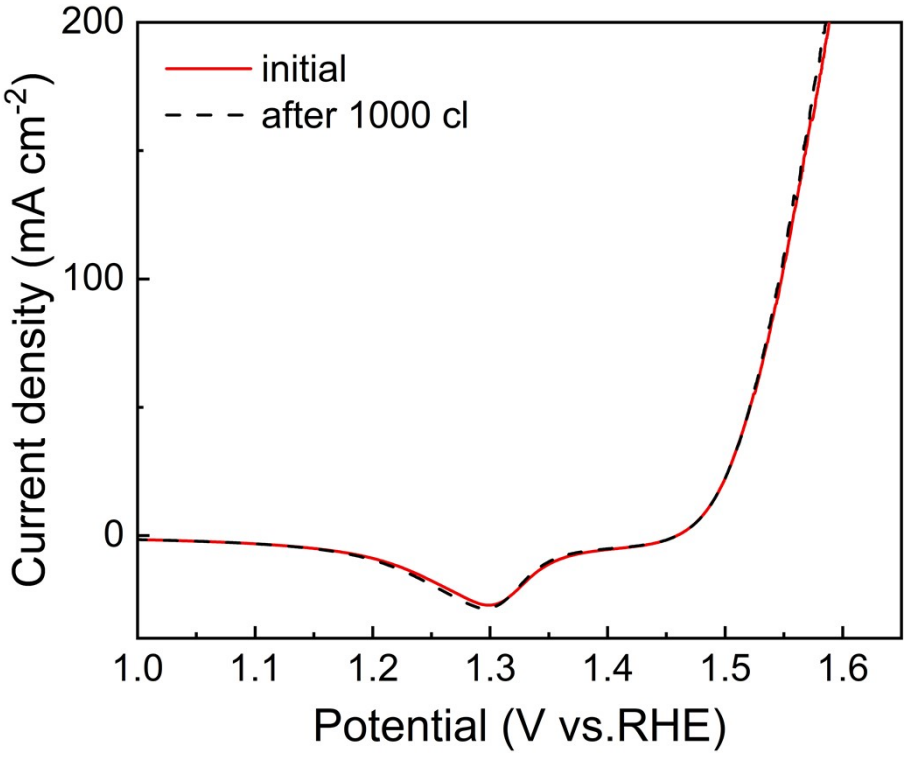

Figure S14. OER polarization curve of $ZnFe_2O_4$@Ni_3S_2/NF initial and after 1000 CV cycles.

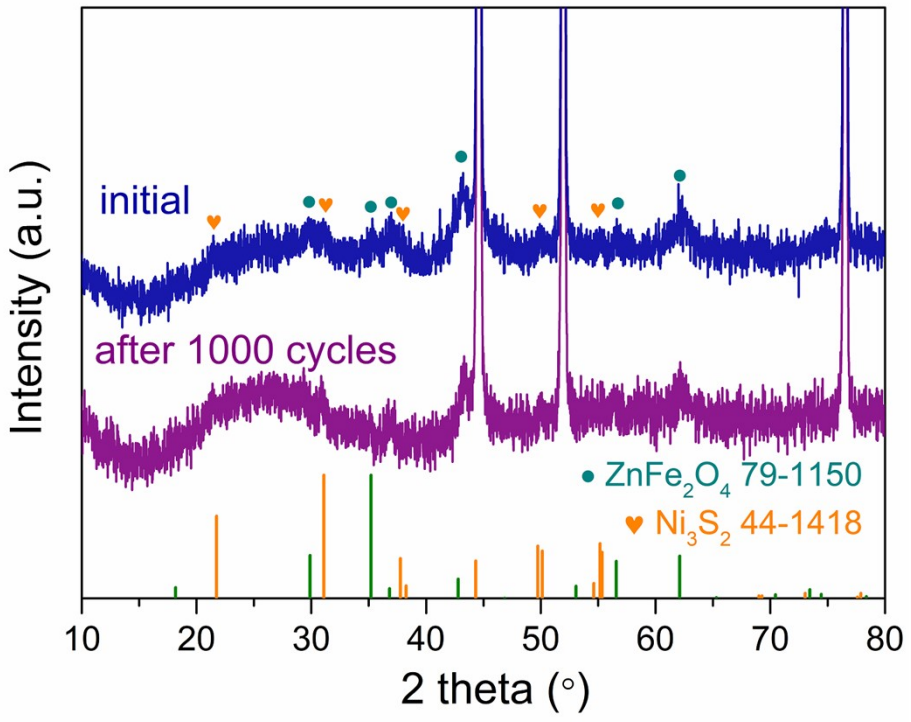

Figure S15. XRD image of $ZnFe_2O_4$@Ni_3S_2/NF initial and after 1000 CV cycles.

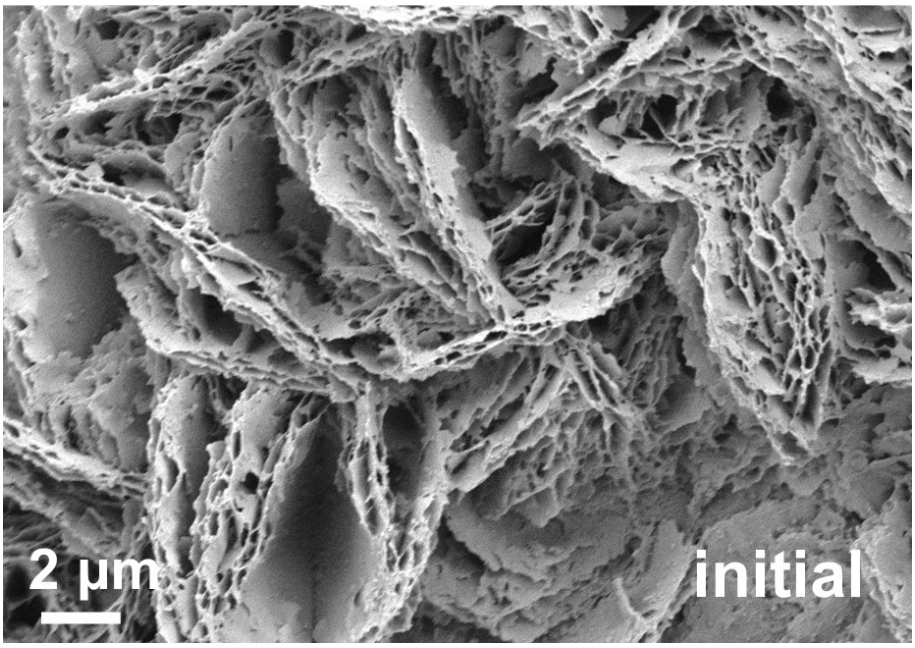

Figure S16. SEM image of $ZnFe_2O_4$@Ni_3S_2/NF initial.

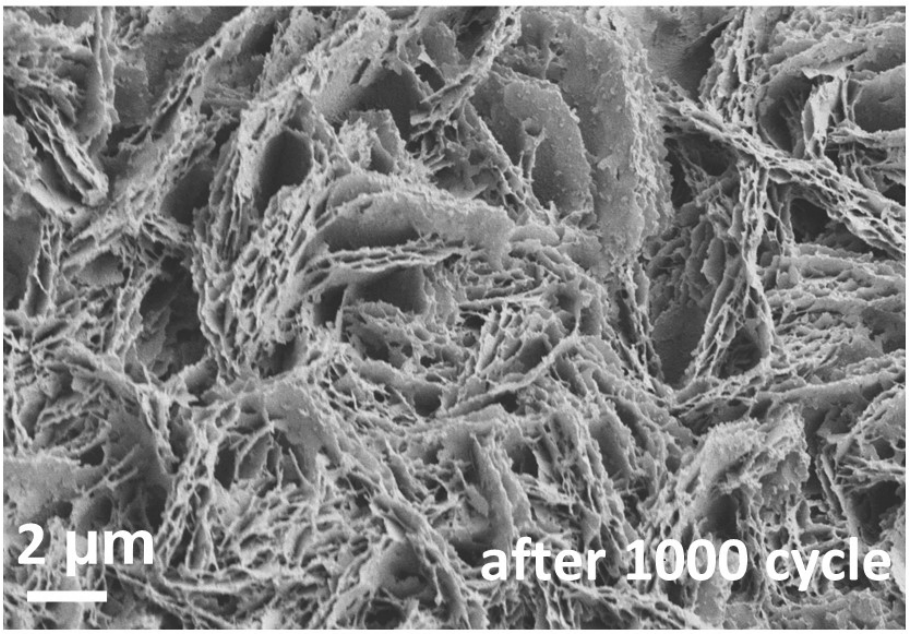

Figure S17. SEM image of $ZnFe_2O_4$@Ni_3S_2/NF after 1000 CV cycle.

Table S1. Comparison of OER performance for $ZnFe_2O_4$@Ni_3S_2/NF with other reported non-noble systems.

Catalysts	Overpotential (mV) at 10 mA cm^{-2}	Tafel solp (mV dec^{-1})	Electrolyte	Ref.
$NiCo_2O_4$@MoS_2/TM	313	66.8	1.0 M KOH	Bao *et al.*[1]
$ZnFe_2O_4$@$ZnFe_2S_4$/NF	320	73	1.0 M KOH	Mohammadpour *et al.*[2]
$ZnFe_{1.25}Al_{0.75}O_4$/NF	270	79	1.0 M KOH	Moon *et al.*[3]
$NiFe_2O_4$/N-graphene	340	93.2	1.0 M KOH	Navadeepthy *et al.*[4]
CoS/$NiFe_2O_4$/NF	227	53	1.0 M KOH	Meng *et al.*[5]
$CoFe_2O_4$/NF	287	43	1.0 M KOH	Lee *et al.*[6]
$SnFe_2O_4$/NF	263	57	1.0 M KOH	Rajput *et al.*[7]
$CuCo_2O_4$-CuO/NF	289	73	1.0 M KOH	Silva *et al.*[8]
NiCo LDH/NiCoS/CC	207	48	1.0 M KOH	Li *et al.*[9]
H-CoS_x@NiFe LDH/NF	250	49	1.0 M KOH	Lee *et al.*[10]
N- Fe_2O_3/$NiTe_2$/NF	253	57.7	1.0 M KOH	Li *et al.*[11]
$ZnFe_2O_4$@Ni_3S_2/NF	254	39.29	1.0 M KOH	This work

References

1. W. W. Bao, Y. Li, J. J. Zhang, T. T. Ai, C. M. Yang and L. L. Feng, *Int. J. Hydrogen Energy*, 2023, **48**, 12176-12184.
2. E. Mohammadpour and K. Asadpour-Zeynali, *Int. J. Hydrogen Energy*, 2021, **46**, 26940-26949.
3. H. Moon, N. Son, M. S. Goh, T. Yoon, J. Kim, C. Liu, Y. Im, S. J. Yoon and M. Kang, *Appl. Surf. Sci.*, 2023, **632**, 12.
4. D. Navadeepthy, A. Rebekah, C. Viswanthan and N. Ponpandian, *Int. J. Hydrogen Energy*, 2021, **46**, 21512-21524.
5. L. X. Meng, H. C. Xuan, G. H. Zhang, R. Wang, J. Wang, Y. Y. Guan, X. Yu, X. H. Liang, Y. P. Li and P. D. Han, *Electrochim. Acta*, 2022, **404**, 10.
6. G. H. Y. Lee, M. Jeong, H. R. Kim, M. Kwon, S. Baek, S. Oh, M. H. Y. Lee, D. J. Lee and J. H. Joo, *ACS Appl. Mater. Interfaces*, 2022, **14**, 48598-48608.
7. A. Rajput, A. A. Pandey, A. Kundu and B. Chakraborty, *Chem. Commun.*, 2023, **59**, 4943-4946.
8. T. R. Silva, R. A. Raimundo, V. D. Silva, J. R. D. Santos, A. J. M. Araújo, J. Oliveira, L. C. de Lima, F. F. da Silva, L. D. Ferreira and D. A. Macedo, *Int. J. Hydrogen Energy*, 2023, **48**, 17160-17176.
9. J. H. Li, L. L. Wang, H. J. He, Y. Q. Chen, Z. R. Gao, N. Ma, B. Wang, L. L. Zheng, R. L. Li, Y. J. Wei, J. Q. Xu, Y. Xu, B. W. Cheng, Z. Yin and D. Ma, *Nano Res.*, 2022, **15**, 4986-4995.
10. Y. J. Lee and S. K. Park, *Small*, 2022, **18**, 10.
11. W. J. Li, Y. Q. Deng, L. Luo, Y. S. Du, X. H. Cheng and Q. Wu, *J. Colloid Interface Sci.*, 2023, **639**, 416-423.